Eur. J. Mineral.
2017, **29**, 679–688
Published online 1 June 2017

Special issue dedicated to Zdeněk Johan

Richardsollyite, $TlPbAsS_3$, a new sulfosalt from the Lengenbach quarry, Binn Valley, Switzerland

NICOLAS MEISSER[1,*], PHILIPPE ROTH[2], FABRIZIO NESTOLA[3], CRISTIAN BIAGIONI[4], LUCA BINDI[5] and MARTIN ROBYR[6]

[1] Musée cantonal de géologie, Université de Lausanne, Anthropole, Dorigny, 1015 Lausanne, Switzerland
*Corresponding author, e-mail: nicolas.meisser@unil.ch
[2] FGL, Swiss Seismological Service, ETH Zurich, Sonneggstr. 5, 8092 Zurich, Switzerland
[3] Dipartimento di Geoscienze, Università di Padova, Via Gradenigo 6, 35131 Padova, Italy
[4] Dipartimento di Scienze della Terra, Università di Pisa, Via S. Maria 53, 56126 Pisa, Italy
[5] Dipartimento di Scienze della Terra, Università degli Studi di Firenze, Via G. La Pira 4, 50121 Firenze, Italy
[6] Institut des sciences de la Terre, Université de Lausanne, Géopolis, Dorigny, 1015 Lausanne, Switzerland

Abstract: The new mineral species richardsollyite, $TlPbAsS_3$, was discovered in the Lengenbach quarry, Imfeld, Binn Valley, Canton Valais, Switzerland, intimately associated with hutchinsonite and baryte. It occurs as grey-black crystals, up to 750 μm, with a metallic lustre. Under the reflected-light microscope, richardsollyite is grey, with bright-red internal reflections; anisotropy is distinct, with greyish-white to bluish rotation tints. Reflectance values for the four COM wavelengths are [R_{min}, R_{max} (%), (λ)]: 27.9, 29.8 (471.1 nm); 27.8, 31.0 (548.3 nm); 27.3, 30.8 (586.6 nm); and 27.0, 30.5 (652.3 nm). Electron microprobe analysis gave (in wt%): Tl 34.72(51), Pb 35.45(20), As 12.80(14), Sb 0.04(1), S 16.22(13), total 99.24(47). On the basis of 6 atoms per formula unit, the chemical formula is $Tl_{1.001}Pb_{1.008}(As_{1.007}Sb_{0.002})_{\Sigma 1.009}S_{2.982}$. The main diffraction lines [d in Å (intensity) hkl] are: 4.23 (80) $\overline{1}$ 0 2; 3.875 (70) $\overline{2}$ 1 1; 3.762 (100) 2 1 0, 1 2 0; 3.278 (70) 1 0 2; 2.931 (70) 0 2 2; 2.714 (70) $\overline{1}$ 1 3; and 2.622 (80) $\overline{3}$ 1 2. Richardsollyite is monoclinic, space group $P2_1/c$, with $a = 8.8925(2)$, $b = 8.4154(2)$, $c = 8.5754(2)$ Å, $\beta = 108.665(3)°$, $V = 607.98(3)$ Å^3, $Z = 4$. The crystal structure was solved and refined to $R_1 = 0.0242$ on the basis of 1590 reflections with $F_o > 4\sigma(F_o)$. It can be described as formed by (1 0 0) $[Pb(AsS_3)]^-$ layers sandwiching Tl^+ cations, and is isostructural with synthetic $ABCX_3$ (A = K, Rb, Cs; B = Eu, Ba; C = As, Sb; X = S, Se) compounds. The new mineral is named after Richard Harrison Solly (1851–1925) for his outstanding contribution to the knowledge of the Lengenbach mineralogy during the first flourishing period of Lengenbach investigations, at the beginning of the 20th Century.

Key-words: richardsollyite; new mineral; sulfosalt; lead; thallium; arsenic; crystal structure; Lengenbach; Binn Valley; Switzerland.

1. Introduction

Thallium displays both chalcophile and lithophile geochemical behaviour, which has resulted in a fascinating range in the mineralogical diversity of this element. Among the 63 known mineral species having Tl as an essential component (as of the end of 2016), 40 belong to the sulfosalt class. In these minerals, thallium either plays the same role as Pb^{2+}, usually replacing it by means of coupled substitutions involving Sb^{3+}, As^{3+} or Bi^{3+}, which replaces neighbouring Pb^{2+}, or is hosted in channels or layers, where it assumes a role similar to that of alkali metals, *e.g.* K^+ (Makovicky, 2005).

The most important locality for the study of Tl sulfosalts is certainly the Lengenbach quarry, Imfeld, Binn Valley, Switzerland, the type locality of 21 Tl-bearing mineral species. In 1905, hutchinsonite (Solly, 1905) was the first Tl mineral to be described from this locality and it represented only the third known Tl mineral worldwide after crookesite (Nordenskiöld, 1866) and lorándite (Krenner, 1894). However, the description of hutchinsonite was based on crystal morphology only, similarly a few years later for hatchite (Solly & Smith, 1912). The chemical nature of hutchinsonite as a Tl mineral was established by Smith & Prior (1907). The other twenty-seven Tl species from Lengenbach were all described in the modern phase of exploitation and investigation (since 1964). A review of the exceptional mineralogy of the Lengenbach deposit is given in Roth *et al.* (2014).

During energy-dispersive X-ray spectrometry (EDXS) screening of a suite of specimens collected in the Lengenbach quarry in 2015 by the Lengenbach Research Association (FGL, the active Lengenbach syndicate), several minerals were set aside for further investigation owing to their unusual characteristics. One of these minerals consisted of Pb, Tl, As and S, in a not yet encountered atomic ratio of approximately 1:1:1:3. Subsequent X-ray diffraction studies and quantitative chemical analyses confirmed that this phase was indeed a new mineral, described here as richardsollyite.

DOI: 10.1127/ejm/2017/0029-2649
0935-1221/17/0029-2649 $ 4.50

The mineral and its name were approved by the CNMNC-IMA (2016-043). The holotype specimen of richardsollyite is deposited in the Mineralogical Collection of the Musée cantonal de géologie, University of Lausanne, Anthropole, Dorigny, 1015 Lausanne, Switzerland, with catalogue number MGL no. 080126.

The name honours Richard Harrison Solly (1851–1925), a British autodidact who carefully described, between 1901 and 1912, eight new mineral species for Lengenbach. He can be considered as the most successful scientist of the first flourishing period of Lengenbach investigations, at the beginning of the 20th Century. However, whereas several scientists of this period have been honoured by giving their name to a Lengenbach mineral (H. Baumhauer, A. Dufrénoy, F.H. Hatch, A. Hutchinson, H. Jordan, G.D. Liveing, J.E. Marr, G. vom Rath, W. Sartorius von Walterhausen, G. Seligmann, G.F.H. Smith, and C.O. Trechmann), Solly is missing in this list. In an effort to assign names to insufficiently characterized minerals, Gagarin & Cuomo (1949), without any investigation and based only on literature data, did give the name "sollyite" to a fibrous sulfosalt from Lengenbach, later discredited by Nowacki *et al.* (1960) as a mixture of two to three different minerals. This happened more than 50 years ago and the name "sollyite" is now available according to the IMA rules (Nickel & Grice, 1998). However, to avoid any confusion with samples previously labelled "sollyite" in old collections, we chose the name richardsollyite for the new mineral species.

This paper reports the description of the new mineral richardsollyite and its crystal structure, together with a discussion of its relationships with a few related synthetic compounds.

2. Occurrence and mineral description

2.1. Occurrence and physical properties

Richardsollyite was collected in cavities of the Triassic metadolostone exposed in the Lengenbach quarry, Imfeld, Binn Valley, Canton Valais, Switzerland (46°21′54″ N, 8°13′15″ E). The mineralized Triassic metadolostone exploited at this locality occurs at the front of the Monte Leone Nappe, in the Penninic domain of the Alps. The Lengenbach deposit has been interpreted to have formed by remobilization of a pre-existing carbonate-hosted Pb–Zn–Ag–Cu–Cd–Tl–As ore deposit and subsequent crystallization from sulphide melt as well as hydrothermal solutions, during Alpine metamorphism under upper greenschist- to lower amphibolite-facies conditions (Hofmann, 1994). This sulphide melt underwent fractional crystallization of sulfosalts such as richardsollyite and associated hutchinsonite, dufrénoysite, wallisite–hatchite series and realgar, which resulted in the enrichment of As and Tl, and the depletion of Pb in the remaining melt fractions. This is shown by compositional trends measured in melt inclusions (Hofmann, 1994), by the presence of more As- and Tl-enriched mineral species in late-stage vugs and veins, and by Tl-isotope fractionation (Hettmann *et al.*, 2014). The presence of a hydrothermal aqueous fluid during and after the crystallization of the sulphide melt was interpreted to be responsible for the re-crystallisation of dolomite and baryte (Hofmann *et al.*, 1993), which are closely associated to richardsollyite in vugs.

Table 1. Species constituting the mineral assemblage of Lengenbach quarry metadolostone Ribbon 1, Zone 1, in which richardsollyite was found. Tl minerals are marked in bold.

"Adularia" and "hyalophane"	**Hutchinsonite**	Rathite
Aktashite	Hydrocerussite	Realgar
Argentobaumhauerite	**Incomsartorite**	**Richardsollyite**
Argentodufrénoysite	**Imhofite**	**Routhierite (?)**
Argentoliveingite	**Jentschite**	Rutile
Arsenic	Jordanite	**Sartorite**
Baryte	Kaolinite	Seligmannite
Baumhauerite	Lengenbachite	Silver
Bernardite	Liveingite	Sinnerite
Canfieldite (Te-rich)	Marrite	Smithite
Cerussite	Muscovite	Sphalerite
Coffinite	Nowackiite	**Stalderite**
Covellite	Orpiment	Tennantite
Dolomite	Pararealgar	**Thalcusite**
Dravite	**Parapierrotite**	Thorite
Dufrénoysite	**Picotpaulite**	Tochilinite
Edenharterite	Proustite	Trechmannite
Erniggliite	Pyrite	Uraninite
Ferrostalderite	Quadratite	**Wallisite**
Galena	Quartz	Wurtzite
Hatchite	**Ralphcannonite**	Xanthoconite

The mineralization occurs in the uppermost part of a 240 m thick metadolostone sequence, 180–200 m above its base, close to the contact with the Jurassic to Lower Cretaceous metapelite locally called "*Bündnerschiefer*". The mineralization in the quarry can be subdivided into four different types according to geometric criteria (Hofmann & Knill, 1996). Using different spatial and geochemical criteria, Graeser *et al.* (2008) distinguished five major, bedding-parallel zones. Richardsollyite, like all the recently described new mineral species, occurs in their realgar-bearing, As- and Tl-rich "Zone 1".

The FGL collected the studied specimen (L-15-6763) in 2015 on level 4. In this extraction area, Zone 1 of Graeser *et al.* (2008) can be further subdivided into isolated, bedding-parallel, mineralized metadolostone ribbons and lenses spaced approximately 1 m apart. Richardsollyite was found in "Ribbon 1", a particularly interesting and well-documented, realgar-rich body. It measured 4 m × 2 m, with a maximum thickness of 0.5 m, and was found to contain a high concentration of rare Tl-rich species. Table 1 summarizes the minerals identified in that volume of metadolostone. The body is sharply separated from the adjacent, poorly mineralized, metadolostone layers. Another mineralized metadolostone ribbon, mined further to the south in the same period, was found to be almost completely Tl-free, even if its realgar concentration – and therefore its apparent As concentration, commonly thought to be correlated to and therefore indicative of Tl – was even higher there than in Ribbon 1.

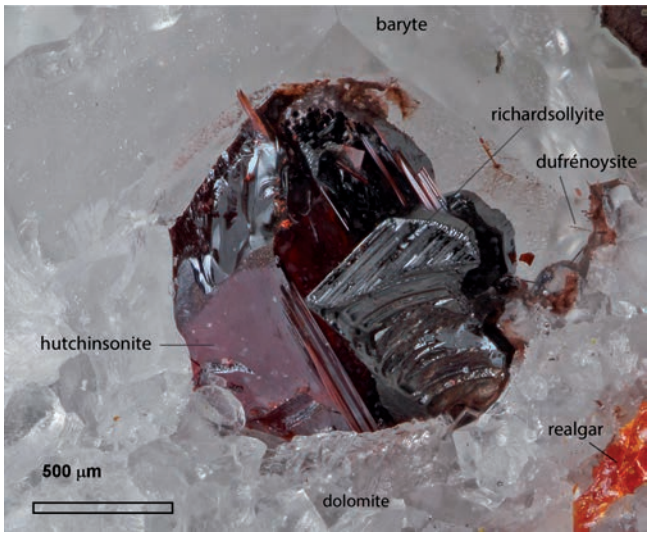

Fig. 1. Metallic grey-black richardsollyite crystals with striated and curved faces have grown on cherry-red hutchinsonite. Associated minerals are Tl-bearing dufrénoysite, in tiny fibrous red-brown needles, orange-red realgar, fine-grained colourless dolomite, and gemmy colourless baryte. Holotype specimen, MGL no. 080126 (L-15-6763).

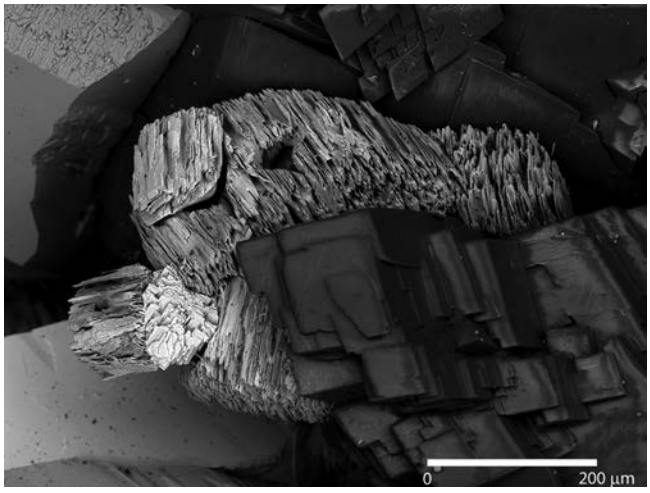

Fig. 2. Backscattered electron image of the second specimen of richardsollyite. It shows stacks of lamellar crystals on dolomite. Oblique terminal faces are discernible in the top left aggregate. Sample specimen no. L-15-6558.

In the specimen studied, richardsollyite forms grey-black euhedral crystals, up to 750 μm across (Fig. 1). The streak is black and the lustre is metallic; it is brittle, with uneven fracture and without any visible cleavage surface. Micro-indentation measurements, carried out with a VHN load of 25 g, give a mean value of 188 kg/mm^2 (range 170–203), corresponding to a Mohs hardness of ~3–3.5. Owing to the rarity and size of richardsollyite, no grain suitable for density measurement was available. The calculated density, based on the empirical formula, is 6.392 g/cm^3; by using the ideal formula, the calculated density is 6.365 g/cm^3.

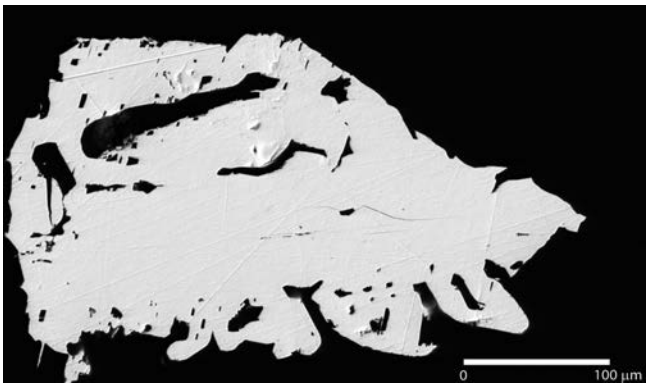

Fig. 3. Backscattered electron image of polished grain of richardsollyite extracted from holotype specimen MGL no. 080126 (L-15-6763). Note the vesicular appearance and the chemical homogeneity.

In plane-polarized incident light, richardsollyite is grey in colour. Under crossed polarisers, it is distinctly anisotropic, with greyish to bluish rotation tints. Internal reflections are bright red. Reflectance measurements were carried out at the Dipartimento di Scienze della Terra, Università degli Studi di Firenze, using a MPM-200 Zeiss microphotometer equipped with a MSP-20 system processor on a Zeiss Axioplan ore microscope. The filament temperature was ~3350 K. An interference filter was adjusted, in turn, to select four COM (IMA Commission on Ore Microscopy) wavelengths for measurements (471.1, 548.3, 586.6, and 652.3 nm). Readings were taken for sample and standard (SiC) maintained under the same focus conditions. The diameter of the circular measuring area was 0.1 mm. Reflectance percentages are [R_{min}, R_{max} (λ in nm)]: 27.9, 29.8 (471.1); 27.8, 31.0 (548.3); 27.3, 30.8 (586.6); and 27.0, 30.5 (652.3). All measurements were done in air.

On the holotype specimen MGL no. 080126 (L-15-6763), richardsollyite is closely associated with hutchinsonite and baryte; other minerals occurring in the same specimen are Tl-bearing dufrénoysite, realgar, pyrite, and dolomite.

Richardsollyite was identified on a second FGL specimen (L-15-6558) from Ribbon 1. Although its EDXS spectrum indicates the absence of detectable trace elements (besides Sb), the physical appearance is different: dark copper-red stacks of tabular to lamellar crystals (Fig. 2) associated with an intermediate member of the hatchite–wallisite solid solution isotypic pair (corresponding to the composition hatchite$_{61}$wallisite$_{39}$), hutchinsonite, probable sartorite, realgar and dolomite.

2.2. Chemical data

A preliminary chemical analysis performed by energy-dispersive spectrometry on a portion of the grain used for the crystal structure study (Fig. 3) did not indicate the presence of elements with $Z > 9$ other than Tl, Pb, As and S. In addition, back-scattered electron images showed the compositional homogeneity of the studied grain.

Table 2. Electron microprobe analysis of richardsollyite: chemical composition as wt% (average of 9 spot analyses) and chemical formula (in atoms per formula unit, apfu) on the basis of 6 apfu.

Element	wt%	Range	e.s.d.	apfu
Tl	34.72	33.92–35.32	0.51	1.001
Pb	35.45	35.07–35.69	0.2	1.008
As	12.8	12.64–13.12	0.14	1.007
Sb	0.04	0.02–0.07	0.01	0.002
S	16.22	16.02–16.44	0.13	2.982
Total	99.23	98.77–99.70	0.47	
Ev*				1.3

* Relative error on the valence equilibrium (%), calculated as $100 \times [\Sigma(\text{val}+) - \Sigma(\text{val}-)]/\Sigma(\text{val}-)$.

Table 3. X-ray powder diffraction data for richardsollyite. Intensities and d_{hkl} (in Å) were calculated using the software *PowderCell* 2.3 (Kraus & Nolze, 1996) on the basis of the structural model given in Table 5. The seven strongest reflections are given in bold. Only reflections with $I_{calc} \geq 10$ were reported.

I_{obs}	d_{obs}	I_{calc}	d_{calc}	$h\,k\,l$	I_{obs}	d_{obs}	I_{calc}	d_{calc}	$h\,k\,l$
		11	5.85	0 1 1			16	2.576	$\bar{2}$ 1 3
80	4.23	51	4.23	$\bar{1}$ 0 2	30	2.462	14	2.457	1 3 1
		14	4.21	2 0 0	40	2.332	28	2.330	3 1 1
70	**3.875**	**93**	**3.866**	**$\bar{2}$ 1 1**	20	2.204	25	2.200	$\bar{2}$ 3 2
		35	3.777	$\bar{1}$ 1 2	20	2.122	12	2.113	$\bar{2}$ 0 4
100	**3.762**	**100**	**3.767**	**2 1 0**			16	2.063	1 2 3
		64	**3.764**	**1 2 0**	30	2.056	14	2.061	$\bar{3}$ 2 3
		36	3.736	0 2 1			14	2.050	$\bar{2}$ 1 4
40	3.633	49	3.619	$\bar{1}$ 2 1	30	2.045	22	2.043	4 1 0
70	**3.278**	**94**	**3.272**	**1 0 2**			11	2.041	1 4 0
		15	3.243	1 2 1			17	1.985	3 3 0
30	3.063	34	3.050	1 1 2	20	1.967	18	1.970	3 1 2
30	2.983	28	2.982	$\bar{1}$ 2 2	20	1.961	17	1.962	$\bar{4}$ 2 1
70	**2.931**	**92**	**2.922**	**0 2 2**			11	1.944	1 4 1
50	2.805	54	2.795	$\bar{3}$ 1 1	30	1.895	22	1.894	$\bar{2}$ 4 1
70	**2.714**	23	2.711	$\bar{2}$ 2 2			19	1.885	2 3 2
		79	**2.707**	**$\bar{1}$ 1 3**			12	1.802	1 1 4
		17	2.664	3 1 0			15	1.770	$\bar{5}$ 0 2
60	2.663	58	2.661	1 3 0			12	1.719	$\bar{4}$ 3 2
		22	2.652	0 3 1			11	1.715	$\bar{3}$ 4 1
		74	**2.622**	**$\bar{3}$ 1 2**			13	1.661	0 4 3
80	**2.622**	62	2.611	2 2 1			12	1.638	$\bar{1}$ 5 1
		17	2.608	$\bar{1}$ 3 1			17	1.614	$\bar{3}$ 3 4

Quantitative chemical analyses of richardsollyite were carried out at Institut des sciences de la Terre, Université de Lausanne, using a JEOL 8200 electron microprobe operating in wavelength-dispersive mode. Experimental conditions were: accelerating voltage 20 kV, beam current 40 nA, focused electron beam. Counting times were 20 s for peak and 10 s for background. Standards (element, emission line) were: lorándite (Tl $M\alpha$, As $L\alpha$), PbS (Pb $M\alpha$, S $K\alpha$), and Sb_2S_3 (Sb $L\alpha$). Fe, Cu, Zn, Ag, and Hg were sought but found to be below the detection limit (0.02 wt%).

Electron microprobe data for richardsollyite are given in Table 2. On the basis of 6 atoms per formula unit (apfu), the chemical formula is $Tl_{1.001}Pb_{1.008}(As_{1.007}Sb_{0.002})_{\Sigma 1.009}S_{2.982}$. The ideal formula is $TlPbAsS_3$, which requires (in wt%) Tl 35.08, Pb 35.56, As 12.86, S 16.51, total 100.00.

2.3. Crystallography

The X-ray powder diffraction pattern of richardsollyite was collected using a 114.6 mm Gandolfi camera with Ni-filtered Cu $K\alpha$ radiation. Elemental Si was used as internal standard. The observed pattern is reported in Table 3, where it is compared with that calculated using the software *PowderCell* (Kraus & Nolze, 1996) using the structural model described below. Owing to the multiple contributions for the majority of the observed reflections, the unit-cell parameters were not refined from X-ray powder diffraction data.

Single-crystal X-ray intensity data collection was carried out at the Dipartimento di Geoscienze, Università di Padova, using a Supernova (Agilent Technologies) diffractometer equipped with the Mova micro-source (spot size 0.120 mm, Mo $K\alpha$) and assembled with a Pilatus 200 K detector (Dectris). A total of 1775 unique reflections were collected.

X-ray diffraction intensity data were integrated and corrected for standard Lorentz-polarization factors with the *CrysAlis RED* (Oxford Diffraction, 2006) software package. Absorption correction was performed using the program *ABSPACK* in *CrysAlis RED* (Oxford Diffraction, 2006). The statistical tests on the distribution of $|E|$ values ($|E^2-1| = 0.867$) and systematic absences suggested the space group symmetry $P2_1/c$. The refined unit-cell parameters are $a = 8.8925(2)$, $b = 8.4154(2)$, $c = 8.5754(2)$ Å, $\beta = 108.665(3)°$, $V = 607.98(3)$ Å^3, $Z = 4$. The a:b:c ratio is 1.0567:1:1.0190.

The structure of richardsollyite was solved by direct methods using *Shelxs*-97 and then refined through *Shelxl*-2014 (Sheldrick, 2015). Scattering curves for neutral atoms were taken from the *International Tables for Crystallography* (Wilson, 1992). After having located the heavier atoms (Pb and Tl sites), the remaining atom positions were found through successive difference-Fourier maps. In the crystal structure of richardsollyite, three cation sites and three anion positions occur. Initially, owing to the similar scattering factors of Pb and Tl, only the scattering curve of the former was used. The site occupation factor (s.o.f.) of the three independent cation positions were refined using the following curves: Pb *vs.* □ for *Me*1 and *Me*2 sites, and As *vs.* □ for *As* site. All cation positions were found fully occupied and their s.o.f. were fixed to 1. Taking into account the bond-valence balance, calculated using the bond-parameters given by Brese & O'Keeffe (1991), *Me*1 and *Me*2 sites were assigned to Tl and Pb, respectively. After several cycles of anisotropic refinement, the agreement factor R_1 converged to 0.0242 for 1590 reflections with $F_o > 4\sigma(F_o)$.

Details of the data collection and crystal structure refinement are given in Table 4.

Table 4. Crystal data and summary of parameters describing data collection and refinement for richardsollyite.

Crystal data	
Crystal size (mm^3)	$0.200 \times 0.100 \times 0.060$
Cell setting, space group	Monoclinic, $P2_1/c$
a (Å)	8.8925(2)
b (Å)	8.4154(2)
c (Å)	8.5754(2)
β (°)	108.665(3)
V ($Å^3$)	607.98(3)
Z	4
Data collection and refinement	
Radiation, wavelength (Å)	Mo $K\alpha$, $\lambda = 0.71073$
Temperature (K)	293
$2\theta_{max}$ (°)	60.06
Measured reflections	16596
Unique reflections	1775
Reflections with $F_o > 4\sigma(F_o)$	1590
R_{int}	0.0576
$R\sigma$	0.0280
Range of h, k, l	$-12 \le h \le 12$ $-11 \le k \le 11$ $-12 \le l \le 12$
R [$F_o > 4\sigma(F_o)$]	0.0242
R (all data)	0.0292
wR (on F^2)	0.0522
GooF	1.051
No. of refined parameters	56
Maximum and minimum residual peak (e, $Å^{-3}$)	2.56 (at 0.73 Å from Tl) −1.94 (at 0.66 Å from Tl)

3. Crystal structure description

Atomic coordinates and displacement parameters are shown in Table 5, whereas Table 6 gives selected bond distances.

3.1. Atom coordination and bond-valence sum

The crystal structure of richardsollyite has three independent cation sites, *i.e.* Pb, Tl, and As, and three S sites. All these sites are located at the general 4*e* position. The Pb site has a distorted bicapped trigonal prismatic coordination, with bond distances ranging between 2.906(2) and 3.451(2) Å, with an average bond distance of 3.122 Å. The bond-valence sum, at the Pb site, is 1.85 valence unit (v.u.). Thallium exhibits seven-fold coordination, with an additional ligand at 3.837(2) Å, giving rise to a distorted bicapped trigonal prism. The seven short Tl–S distances range between 3.111(2) and 3.570(2) Å, with average ⟨Tl–S⟩ of 3.333 Å. The bond-valence sum is 1.21 v.u. The slight oversaturation at the Tl site, coupled with the slight underbonding at the Pb position, could be interpreted as due to a partial substitution of Tl at the Pb site and *vice versa*. Actually, Biagioni *et al.* (2014a) pointed out that the bond parameter for the pair (Tl,S) tabulated by Brese & O'Keeffe (1991) is likely overestimated, suggesting the use of a value around 2.55 Å. By using this value, the bond-valence sum at the Tl is lowered to 0.98 v.u. Consequently, the undersaturation at the Pb site could also be related to experimental errors or to the inadequacy of the ionic model used to describe this covalent compound. Arsenic displays a typical trigonal pyramidal coordination, with average ⟨As–S⟩ distance of 2.258 Å and distances ranging between 2.246(2) and 2.274(2) Å. The corresponding bond-valence sum is 3.01 v.u.

Sulfur atoms display different bond environments. S1 is five-fold coordinated, with a square pyramidal coordination. The As site occupies the pyramidal apex, with a short 2.246(2) Å distance, whereas the base has two Pb and two Tl atoms, at distances ranging from 3.004(2) to 3.115(2) Å. A sixth bond involves a Tl atom located at 3.570(2) Å, giving rise to a distorted octahedral coordination. The bond-valence sum at the S1 atom is 2.20 v.u. A similar bonding environment is shown by the S2 site. In this case, S2 is bonded to As (at 2.274 Å) and four Pb atoms, at distances ranging between 3.040(2) and 3.229 (2) Å. The coordination is completed by a sixth Tl atom at 3.433(2) Å. The bond-valence sum, at the S2 site, is 1.91 v.u. Finally, S3 is coordinated by As, two Pb, and two Tl atoms; an additional Tl atom is at a very long distance, 3.837(2) Å. The bond-valence sum, calculated taking into account *Me*–S distances shorter than 3.60 Å, is 1.92 v.u.

3.2. Crystal structure of richardsollyite

The crystal structure of richardsollyite can be described as having (1 0 0) $[Pb(AsS_3)]^-$ layers sandwiching Tl^+ cations (Fig. 4a, b).

The PbS_8 polyhedra share rectangular faces and edges to form chains along *b*; the sharing of rectangular faces gives rise to Pb–Pb distances of 3.744(1) Å. These chains are connected along *c* through sharing the triangular faces of the trigonal prismatic coordination polyhedra of Pb. The AsS_3 trigonal pyramids decorate the polyhedral layer formed by Pb atoms on both sides, giving rise to the (1 0 0) $[Pb(AsS_3)]^-$ layers. These layers are connected along [1 0 0] through Tl–S bonds.

This kind of structure is new for natural sulfosalts, whereas it is isostructural with a few synthetic compounds.

4. Discussion

4.1. Richardsollyite in the framework of lead–thallium sulfosalts

Richardsollyite is the fifteenth natural Tl–Pb sulfosalt and the sixth having a (Tl/Pb) atomic ratio of 1 (Table 7). It is impressive that eleven of these have their type locality in Lengenbach: hutchinsonite (Solly, 1905), edenharterite (Graeser & Schwander, 1992), jentschite (Graeser & Edenharter, 1997), the isotypic pair hatchite–wallisite (Solly & Smith, 1912; Nowacki, 1965), dalnegroite (Nestola *et al.*, 2009), and the recently defined minerals enneasartorite, hendekasartorite, heptasartorite, and incomsartorite (Topa *et al.*, 2016b, 2017a, this issue). The other four were first described from Jas Roux, Hautes-Alpes, France (chabournéite – Johan *et al.*, 1981; écrinsite

Table 5. Atomic fractional coordinates and displacement parameters (Å^2) for richardsollyite.

Site	*x*	*y*	*z*	U^{11}	U^{22}	U^{33}	U^{23}	U^{13}	U^{12}	U_{eq}
Tl	0.41635(3)	0.41732(4)	0.78403(4)	0.0291(2)	0.0343(2)	0.0336(2)	−0.0049(1)	0.0081(1)	−0.0060(1)	0.0328(1)
Pb	0.91460(3)	0.29496(3)	0.98230(3)	0.0262(1)	0.0186(1)	0.0289(1)	0.0036(1)	0.0108(1)	−0.0008(1)	0.0241(1)
As	0.75779(7)	0.55112(7)	0.62970(7)	0.0230(3)	0.0148(3)	0.0169(3)	0.0041(2)	0.0046(2)	0.0026(2)	0.0186(1)
S1	0.7371(2)	0.6012(2)	0.8792(2)	0.0219(7)	0.0191(7)	0.0232(7)	−0.0051(6)	0.0079(6)	0.0015(6)	0.0212(3)
S2	0.0211(2)	0.4913(2)	0.7176(2)	0.0182(7)	0.0242(8)	0.0182(7)	−0.0044(6)	0.0055(5)	−0.0037(6)	0.0203(3)
S3	0.6498(2)	0.3060(2)	0.5876(2)	0.0214(8)	0.0233(8)	0.0409(10)	−0.0151(7)	0.0124(7)	−0.0057(6)	0.0280(4)

Table 6. Selected bond distances (in Å) for richardsollyite.

Tl	–S1	3.111(2)	Pb	–S3	2.906(2)	As	–S1	2.246(2)
	–S1	3.115(2)		–S1	3.004(2)		–S3	2.255(2)
	–S3	3.203(2)		–S2	3.040(2)		–S2	2.274(2)
	–S3	3.340(2)		–S1	3.068(2)		Mean	2.258
	–S2	3.433(2)		–S2	3.090(2)			
	–S3	3.560(2)		–S2	3.186(2)			
	–S1	3.570(2)		–S2	3.229(2)			
				–S3	3.451(2)			
	Mean	3.333		Mean	3.122			

– Topa *et al.*, 2017b), and from the Monte Arsiccio mine, Tuscany, Italy (boscardinite – Orlandi *et al.*, 2012; protochabournéite – Orlandi *et al.*, 2013). Among Pb–Tl sulfosalts, richardsollyite is richest in (Pb + Tl), with a [(Pb + Tl)/As] atomic ratio of 2; in the other known sulfosalts, this ratio is ≤1.

In sulfosalt systematics, two different crystal-chemical behaviours of Tl have been observed in Pb–Tl sulfosalts (Moëlo *et al.*, 2008):

i) Tl^+ replacing Pb^{2+}, both as a minor component or as an essential constituent. In this case, the introduction of Tl^+ is related to an increase of Me^{3+} (usually As or Sb) content, according to the substitution mechanism $Tl^+ + Me^{3+} = 2Pb^{2+}$;

ii) Tl and Pb occurring at different positions.

Case *i* is represented by minerals derived from Tl-free, Pb end-members. As an example, boscardinite is the Tl–Sb homeotype of the pure Pb–As sulfosalt baumhauerite (Orlandi *et al.*, 2012; Biagioni & Moëlo, 2017a). In this mineral, thallium occurs in pure Tl or mixed (Tl/Pb) positions, with a pure Tl site having a tricapped trigonal prismatic coordination. The average ⟨Tl–S⟩ distance is 3.36–3.37 Å. Écrinsite, a new mineral species recently described by Topa *et al.* (2017b), displays similar features as the new sartorite homeotypes (Topa *et al.*, 2017a). A significant Tl–Pb substitution is also shown by members of the chabournéite series (chabournéite, dalnegroite, and protochabournéite), with Tl usually occurring in bonding environments similar to those observed in boscardinite. The occurrence of non-negligible amounts of Tl in Pb sulfosalts is well-known, having been reported in dufrénoysite and rathite (Laroussi *et al.*, 1989; Berlepsch *et al.*, 2002; Moëlo *et al.*, 2008), as well as, more recently, in the oxy-sulfosalts rouxelite and chovanite (Biagioni *et al.*, 2014b; Biagioni & Moëlo, 2017b).

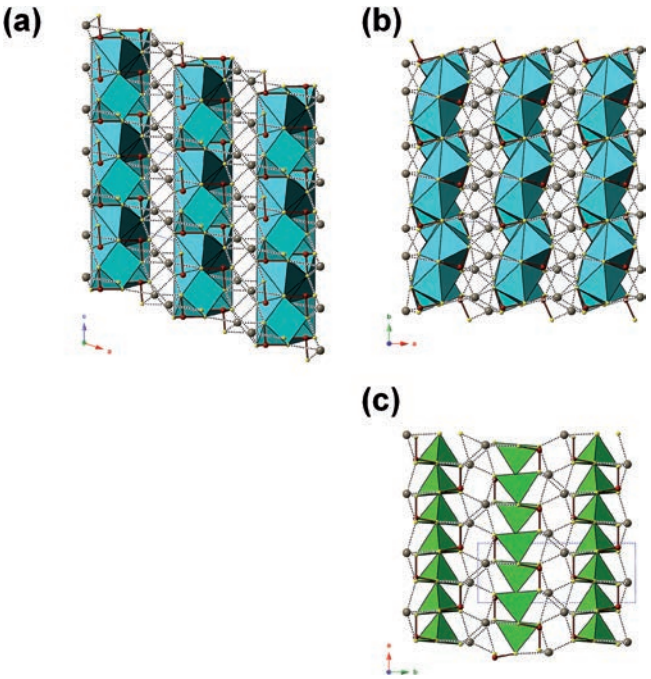

Fig. 4. Crystal structure of richardsollyite as seen down **b** (a) and **c** (b). Light blue polyhedra represent the Pb site. Tl and As sites are represented as grey and red ball-and-sticks, respectively and S as yellow circles. For sake of comparison, the crystal structure of christite (c), as seen down **c**, is shown. Same symbols as in (a) and (b) for Tl, As, and S sites; green polyhedra represent the Hg site.

Case *ii* is well exemplified by members of the hutchinsonite merotypic series hutchinsonite, edenharterite, and jentschite (*e.g.* Makovicky, 1997). Indeed, Tl and Pb are partitioned into different sites, with different average bond distances. In the eponymous mineral hutchinsonite, Pb is seven-fold coordinated, with ⟨Pb–S⟩ of 3.06 Å whereas Tl has seven short Tl–S distances and three longer ones, with average ⟨Tl–S⟩ distances of 3.45 Å (Matsushita & Takéuchi, 1994). In the pair edenharterite–jentschite, Berlepsch (1996) gave ⟨Pb–S⟩ of 3.07–3.08 Å and ⟨Tl–S⟩ of 3.31 Å. Both elements have seven shorter (= stronger) *Me*–S bonds, but Tl displays two additional longer (= weaker) bonds. The crystal structures of the isotypic pair hatchite–wallisite were studied by Marumo & Nowacki (1967) and by Takéuchi & Ohmasa (1968). Later, Boiocchi & Callegari (2003) studied an intermediate member in the hatchite–wallisite solid solution. Also in these minerals Pb and Tl are partitioned in two different eight-fold coordinated sites, having average ⟨Pb–S⟩ and ⟨Tl–S⟩ distances of 3.10 and 3.44 Å (Boiocchi & Callegari, 2003), respectively.

Table 7. Unit-cell parameters, space group and chemical formula of lead–thallium sulfosalt species.

Mineral species	*a* (Å)	*b* (Å)	*c* (Å)	α (°)	β (°)	γ (°)	s.g.	Chemical formula	Ref.
Boscardinite	8.09	8.76	22.50	90.9	97.2	90.8	$P\bar{1}$	$TlPb_4(Sb,As)_9S_{18}$	[1]
Chabournéite	8.52	42.46	16.29	83.4	91.0	84.3	*P*1	$Tl_2Pb(Sb,As)_{10}S_{17}$	[2]
Dalnegroite	16.22	42.55	8.56	95.7	90.2	96.4	*P*1	$Tl_2Pb(As,Sb)_{10}S_{17}$	[3]
Écrinsite	8.08	8.53	22.61	90.2	97.2	90.8	$P\bar{1}$	$AgTl_3Pb_4As_{11}S_9S_{36}$	[4]
Edenharterite	15.48	47.60	5.85	90	90	90	*Fdd*2	$TlPbAs_3S_6$	[5]
Enneasartorite	37.61	7.88	20.07	90	101.9	90	$P2_1/b$	$Tl_6Pb_{32}As_{70}S_{140}$	[6]
Hatchite	8.04	9.17	7.81	105.2	113.6	64.8	$P\bar{1}$	$AgTlPbAs_2S_5$	[7]
Hendekasartorite	31.81	7.89	28.56	90	99.0	90	$P2_1/b$	$Tl_2Pb_{48}As_{82}S_{172}$	[6]
Heptasartorite	29.27	7.88	20.13	90	102.1	90	$P2_1/b$	$Tl_7Pb_{22}As_{55}S_{108}$	[6]
Hutchinsonite	10.79	35.39	8.14	90	90	90	*Pbca*	$TlPbAs_5S_9$	[8]
Incomsartorite	45.99	7.87	58.67	90	90.15	90	$P2_1/n$	$Tl_6Pb_{144}As_{246}S_{516}$	[9]
Jentschite	8.10	23.92	5.89	90	108.1	90	$P2_1/n$	$TlPbAs_2SbS_6$	[5]
Protochabournéite	8.15	8.72	21.58	85.2	96.9	88.6	$P\bar{1}$	$Tl_2Pb(Sb,As)_{10}S_{17}$	[10]
Richardsollyite	8.89	8.42	8.58	90	108.7	90	$P2_1/c$	$TlPbAsS_3$	[11]
Wallisite	7.98	8.97	7.76	106.1	114.5	65.5	$P\bar{1}$	$CuTlPbAs_2S_5$	[12]

[1] Orlandi *et al.* (2012); [2] Biagioni *et al.* (2015); [3] Bindi *et al.* (2010); [4] Topa *et al.* (2017b); [5] Berlepsch (1996); [6] Topa *et al.* (2017a); [7] Marumo & Nowacki (1967); [8] Matsushita & Takéuchi (1994); [9] Topa *et al.* (2016b); [10] Orlandi *et al.* (2013); [11] this work; [12] Takéuchi & Ohmasa (1968).

Table 8. Synthetic isotypic analogues of richardsollyite.

Compound	*a* (Å)	*b* (Å)	*c* (Å)	β (°)	*V* (Å^3)	s.g.	Ref.
Richardsollyite	8.892	8.415	8.575	108.66	607.98	$P2_1/c$	[1]
$KEuAsS_3$	8.831	8.346	8.622	106.59	608.98	$P2_1/c$	[2]
$RbEuAsS_3$	9.080	8.367	8.675	105.84	633.99	$P2_1/c$	[2]
$CsEuAsS_3$	9.395	8.441	8.770	105.12	671.40	$P2_1/c$	[2]
$KBaAsSe_3$	9.369	9.049	9.247	108.23	744.60	$P2_1/c$	[3]
$KBaSbSe_3$	9.386	9.199	9.369	108.25	768.30	$P2_1/c$	[3]

[1] This work; [2] Bera & Kanatzidis (2008); [3] Yin *et al.* (2014).

Richardsollyite represents a new example among Pb–Tl sulfosalts of crystal-structure partitioning of these two metals.

4.2. Relationships with natural $A^+B^{2+}C^{3+}S_3$ minerals and synthetic analogues

Richardsollyite is a new example of $A^+B^{2+}C^{3+}S_3$ compound among natural sulfosalts. Balić-Žunić & Bente (1995) stressed the role of the *A* cation in controlling the type of crystal structure shown by these ternary compounds. Among the fifteen known sulfosalts having such a formula, the A^+ cation is represented by Tl (christite, richardsollyite), Cu (members of the isotypic series of bournonite and of mückeite, as well as aikinite), and Ag (in the freislebenite series and the related isotypic pair manganoquadratite–quadratite, as well as in laffittite). Christite, $TlHgAsS_3$, the only other ternary sulfosalt with Tl as the A^+ cation, shows some similarity with richardsollyite. Indeed, they have a similar unit-cell volume, *i.e.* 601 and 608 Å^3 in christite and richardsollyite, respectively, and a similar atomic stacking along *b* of christite and *a* of richardsollyite (Fig. 4c). Brown & Dickson (1976) described the crystal structure of christite as formed by two-dimensional $[Hg(AsS_3)]^-$ sheets, bonded together by Tl–S bonds. Whereas the Hg coordination induces the presence of a symmetry plane in the $[B^{2+}(C^{3+}S_3)]^-$ sheet of christite, the lone-electron-pair activity of Pb^{2+} gives rise to an asymmetric coordination without any symmetry plane parallel to the sheets in richardsollyite.

Synthetic $TlPbAsS_3$ was reported by Cai (1984), but its crystal structure was not solved. In contrast, Balić-Žunić & Bente (1995) studied synthetic $TlPbSbS_3$ and solved its crystal structure on the basis of X-ray powder diffraction data. This synthetic compound occurs in two polymorphs, *i.e.* a high-*T* orthorhombic *Cmcm* phase and a low-*T* monoclinic $P2_1/c$ dimorph. The latter has the unit-cell parameters $a = 4.17$, $b = 4.29$, $c = 12.16$ Å, $\beta = 105.5°$, $V = 209.4$ Å^3. Its crystal structure is characterized by tightly bonded double-layers of atoms, with deformed semi-octahedral coordinations. The atomic double-layers are stacked along *c* through longer *Me*–S bonds. This structure could be an average structure, as indicated by the cation disorder, with Tl, Pb, and Sb occupying the same site. It is likely that these cations would be ordered in the true structure, as observed for Tl, Pb, and As in richardsollyite.

Thus, the crystal structure displayed by richardsollyite is new among sulfosalts, but it has been observed in some synthetic alkali sulfosalts (Table 8). Indeed, Bera & Kanatzidis (2008) synthesized three Eu compounds in molten alkali-metal polysulphide salts, having the compositions $KEuAsS_3$, $RbEuAsS_3$, and $CsEuAsS_3$. These compounds display the same structure type as richardsollyite, *i.e.* (1 0 0) $[Eu(AsS_3)]^-$ layers sandwiching A^+ ions, where $A = (K, Rb, Cs)$.

The unit-cell volume of richardsollyite is close to that of $KEuAsS_3$, *i.e.* 607.98 *vs.* 608.98 Å^3. In order to compare their observed and theoretical unit-cell volumes, these two compounds can be considered as mixtures of the simple sulphides $Tl_2S + Pb_2S_2 + As_2S_3$ and $K_2S + Eu_2S_2 + As_2S_3$, respectively. The volume of Tl_2S ($V = 86.13$ Å^3) is larger than that of K_2S ($V = 79.36$ Å^3), whereas Pb_2S_2 ($V = 104.48$ Å^3) is slightly smaller than Eu_2S_2 ($V = 106.43$ Å^3). The volume of As_2S_3 is 116.92 Å^3. Thus,

the unit-cell volume of ½ ($Tl_2Pb_2As_2S_6$) is calculated as 153.77 Å^3, to be compared with the observed one, *i.e.* 152.00 Å^3; the unit-cell volume of ½ ($K_2Eu_2As_2S_6$) is calculated as 151.36 Å^3, whereas the measured one is 152.25 Å^3. Consequently, the predicted unit-cell volume of richardsollyite (152.00 × 4 Å^3) ought to be just a little larger than that of $KEuAsS_3$. Possibly, the small contraction of the measured volume of richardsollyite relative to the predicted one could be due to the lone-electron-pair activity of Tl^+ and Pb^{2+}. Among these isotypic compounds, richardsollyite shows the smallest unit-cell volume, which results from a shorter *c* parameter and a larger β angle compared to its isostructural compounds.

Yin *et al.* (2014) synthesized two seleniosalts with the compositions $KBaAsSe_3$ and $KBaSbSe_3$. Unit-cell volumes are significantly larger than those of the corresponding Eu and Pb counterparts, owing to the large volume of Ba_2S_2 (V = 130.28 Å^3) and to the Se-to-S substitution. In addition, Yin *et al.* (2014) pointed out that, whereas K is eight-fold coordinated in $KEuAsS_3$, it is seven-fold coordinated in the synthetic phases studied by them. Indeed, K–Se distances range between 3.27 and 3.79 Å in the As compound; an eighth Se atom is located at 4.14 Å. Consequently, the coordination of K in $KBaAsSe_3$ (as well as in $KBaSbSe_3$) is similar to that observed in richardsollyite, where Tl has seven short bonds and an additional longer bond.

4.3. Thallium and alkaline metals in natural chalcogenides

The isostructurality between richardsollyite and some synthetic alkali sulfosalts reminds us about the occurrence of other isostructural minerals showing Tl–alkali substitution. Potassium chalcogenides are exceptional minerals, which are limited to the very peculiar geological environments usually represented by alkaline rocks.

Bukovite, $Tl_2(Cu,Fe)_4Se_4$, murunskite, $K_2(Cu,Fe)_4S_4$, and thalcusite, $Tl_2Cu_3FeS_4$, belong to the bukovite group, a series of tetragonal sulphides and selenides of Cu and Fe with Tl and/or K showing a layered structure, with (0 0 1) layers of edge-sharing (Cu,Fe)-centred tetrahedra alternating with layers of eight-fold coordinated (K,Tl) (*e.g.* Makovicky *et al.*, 1980; Pekov *et al.*, 2009). A solid solution between thalcusite and murunskite is suggested by the occurrence of Tl-rich murunskite in the Palitra peralkaline pegmatite, Mount Kedykverpakhk, Lovozero alkaline massif, Russia (Pekov & Agakhanov, 2008).

Another interesting group of sulphides is represented by the isostructural picotpaulite, $TlFe_2S_3$, rasvumite, KFe_2S_3, and pautovite, $CsFe_2S_3$; these minerals can also be enriched in Rb, as reported by Chakhmouradian *et al.* (2007) for rasvumite occurring in sodalite syenite from Mont Saint-Hilaire, Québec, Canada. Their crystal structures have [0 0 1] double chains of edge-sharing Fe-centred tetrahedra interconnected by ten-fold coordinated Tl atoms which form zig–zag chains along *c* (*e.g.* Balić-Žunić *et al.*, 2008).

The most widespread alkali sulphide is probably represented by djerfisherite, $K_6Fe_{25}S_{26}Cl$. On the contrary, its Tl-analogue, thalfenisite, $Tl_6Fe_{25}S_{26}Cl$, is described from only one locality, *i.e.* the Oktyabr'skoe Cu–Ni deposit in Norilsk, eastern Siberia, Russia. A third compound, "Cu–djerfisherite" has been described, but not formally approved, as a different mineral species (Azarova *et al.*, 2006). In addition, Cl-poor analogues of these minerals have been reported (Barkov *et al.*, 1997). The crystal structure of djerfisherite (Dmitrieva *et al.*, 1979) can be considered a derivative of the pentlandite structure. Potassium, as well as Tl, is hosted within structural channels. A short review of the crystal structures of this mineral group is given in Makovicky (2005).

Among sulfosalts, thallium–alkali substitutions are known in the homeotypic pair gillulyite–ambrinoite, with the compositions $Tl_2(As,Sb)_8S_{13}$ and $(K,NH_4)_2(As,Sb)_8S_{13}$, respectively. Their crystal structures show $[(As,Sb)_8S_{13}]^{2-}$ slabs, with Tl and K (the latter being coordinated also by H_2O groups) hosted within inter-slab spaces (Makovicky & Balić-Žunić, 1999; Biagioni *et al.*, 2011).

Galkhaite, ideally $(Hg_5Cu)CsAs_4S_{12}$ (Biagioni *et al.*, 2014c), is the only Cs sulfosalt known to date; it is an example of a cage-like chalcogenide, with Cs hosted in the twelve-fold coordinated cavities of a tetrahedrite-like skeleton (Makovicky, 2005). In a few cases, Tl has been found as a minor component replacing Cs, but Chen & Szymański (1981) reported chemical analyses with Tl > Cs, which pointed to the possible existence of a Tl-dominant analogue. Such a Tl analogue of galkhaite was recently approved as vorontsovite, $(Hg_5Cu)TlAs_4S_{12}$ (Kasatkin *et al.*, 2016).

Other Tl–K substitutions in minerals are known, *e.g.* in chalcothallite, $Tl_2(Cu,Fe)_6SbS_4$, containing 0.8 wt% K (Makovicky *et al.*, 1980).

Taking into account such a widespread Tl–K substitution in chalcogenides, the description of richardsollyite and its relationships with synthetic analogues allow us to predict the existence of natural alkali analogues, *e.g.* $KPbAsS_3$, especially in hyperalkaline geochemical environments, such as, igneous alkaline rocks and marine and non-marine metaevaporites.

5. Conclusion

Richardsollyite is a new Pb–Tl sulfosalt showing the highest (Pb + Tl)/As atomic ratio reported to date. In the past two years ten new mineral species have been described from the Lengenbach quarry. They all are structurally related to existing species: eckerite (Bindi *et al.*, 2015a) to xanthoconite and pyrostilpnite; ralphcannonite and ferrostalderite (Bindi *et al.*, 2015b; Biagioni *et al.*, 2016) to the existing members of the routhierite isotypic series; argentobaumhauerite (Topa & Makovicky, 2016), argentodufrénoysite and argentoliveingite (Topa *et al.*, 2016a and c) to their Ag-free counterparts, and four new sartorites (Topa *et al.*, 2016b, 2017a, this issue) to the existing members of the sartorite homologous series. By contrast, the crystal structure of the new mineral species richardsollyite described in this paper is new in nature, being previously known only in some synthetic alkali sulfosalts.

This study underlines the importance and the uniqueness of the Lengenbach deposit for the study of Tl mineralogy. This locality represents a natural laboratory where subtle geochemical variations in the crystallization medium gave rise to a remarkable and sometimes unpredictable variety of mineral species.

Acknowledgements: We greatly appreciate the field support of Ralph Cannon for his careful extraction and examination of samples from the Lengenbach deposit. Stefan Ansermet is thanked for his photography. We thank Edward Grew and Chris Stanley for helping us in improving the manuscript. The authors are particularly grateful to an anonymous reviewer for his constructive and very helpful comments.

References

Azarova, Yu.V., Krinov, D.I., Sokolova, M.N. (2006): Structural and genetic relationship of djerfisherite and bartonite and problem of isomorphism in the system djerfisherite–"Cu-djerfisherite"–bartonite. *Novye Dannye o Mineralakh [New Data Miner.]*, **41**, 98–107.

Balić-Žunić, T. & Bente, K. (1995): The two polymorphs of $TlPbSbS_3$ and the structural relations of phases in the system $TlSbS_2$–PbS. *Mineral. Petrol.*, **53**, 265–276.

Balić-Žunić, T., Karanović, L., Poleti, D. (2008): Crystal structure of picotpaulite, $TlFe_2S_3$, from Allchar, FYR Macedonia. *Acta Chim. Slov.*, **55**, 801–809.

Barkov, A.Y., Laajoki, K.V.O., Gehör, S.A., Yakovlev, Y.N., Taikina-Aho, O. (1997): Chlorine-poor analogues of djerfisherite-thalfenisite from Noril'sk Siberia and Salmagorsky, Kola Peninsula, Russia. *Can. Mineral.*, **35**, 1421–1430.

Bera, T.K. & Kanatzidis, M.G. (2008): $AEuAsS_3$ (A = Li, K, Rb, and Cs): new As^{3+} species from an arsenic-rich polysulfide flux. *Inorg. Chem.*, **47**, 7068–7070.

Berlepsch, P. (1996): Crystal structure and crystal chemistry of the homeotypes edenharterite ($TlPbAs_3S_6$) and jentschite ($TlPbAs_2SbS_6$) from Lengenbach, Binntal (Switzerland). *Schweiz. Mineral. Petrogr. Mitt.*, **76**, 147–157.

Berlepsch, P., Armbruster, T., Topa, D. (2002): Structural and chemical variations in rathite, $Pb_8Pb_{4-x}(Tl_2As_2)_x(Ag_2As_2)As_{16}S_{40}$: modulations of a parent structure. *Z. Kristallogr.*, **217**, 581–590.

Biagioni, C. & Moëlo, Y. (2017a): Lead-antimony sulfosalts from Tuscany (Italy). XVIII. New data on the crystal-chemistry of boscardinite. *Mineral. Mag.*, **81**, 47–60.

—, — (2017b): Lead-antimony sulfosalts from Tuscany (Italy). XIX. Crystal-chemistry of chovanite from two new occurrences in Apuan Alps and its 8 Å crystal structure. *Mineral. Mag.*, **81**, doi:10.1180/minmag.2016.080.134.

Biagioni, C., Bonaccorsi, E., Pasero, M., Moëlo, Y., Ciriotti, M.E., Bersani, D., Callegari, A.M., Boiocchi, M. (2011): Ambrinoite, $(K,NH_4)_2(As,Sb)_8S_{13}\cdot H_2O$, a new mineral from Upper Susa Valley, Piedmont, Italy: the first natural (K,NH_4)-hydrated sulfosalt. *Am. Mineral.*, **96**, 878–887.

Biagioni, C., Bonaccorsi, E., Moëlo, Y., Orlandi, P., Bindi, L., D'Orazio, M., Vezzoni, S. (2014a): Mercury-arsenic sulfosalts from the Apuan Alps (Tuscany, Italy). II. Arsiccioite, $AgHg_2TlAs_2S_6$, a new mineral from the Monte Arsiccio mine: occurrence, crystal structure and crystal chemistry of the routhierite isotypic series. *Mineral. Mag.*, **78**, 101–117.

Biagioni, C., Moëlo, Y., Orlandi, P. (2014b): Lead-antimony sulfosalts from Tuscany (Italy). XV. (Tl–Ag)-bearing rouxelite from Monte Arsiccio mine: occurrence and crystal chemistry. *Mineral. Mag.*, **78**, 651–661.

Biagioni, C., Bindi, L., Zaccarini, F. (2014c): Crystal chemistry of mercury sulfosalts – Galkhaite, $(Hg_{5+x}Cu_{1-x})Cs_{1-x}As_4S_{12}$ ($x \approx 0$): crystal structure and revision of the chemical formula. *Can. Mineral.*, **52**, 873–882.

Biagioni, C., Moëlo, Y., Favreau, G., Bourgoin, V., Boulliard, J.-C. (2015): Structure of Pb-rich chabournéite from Jas Roux, France. *Acta Crystallogr.*, **B71**, 81–88.

Biagioni, C., Bindi, L., Nestola, F., Cannon, R., Roth, P., Raber, T. (2016): Ferrostalderite, $CuFe_2TlAs_2S_6$, a new mineral from Lengenbach, Switzerland: occurrence, crystal structure, and emphasis on the role of iron in sulfosalts. *Mineral. Mag.*, **80**, 175–186.

Bindi, L., Nestola, F., Guastoni, A., Secco, L. (2010): The crystal structure of dalnegroite, $Tl_{5-x}Pb_{2x}(As, Sb)_{21-x}S_{34}$: a masterpiece of structural complexity. *Mineral. Mag.*, **74**, 999–1012.

Bindi, L., Nestola, F., Graeser, S., Tropper, P., Raber, T. (2015a): Eckerite, Ag_2CuAsS_3, a new Cu-bearing sulfosalt from Lengenbach quarry, Binn valley, Switzerland: description and crystal structure. *Mineral. Mag.*, **79**, 687–694.

Bindi, L., Biagioni, C., Raber, T., Roth, T., Nestola, F. (2015b): Ralphcannonite, $AgZn_2TlAs_2S_6$, a new mineral of the routhierite isotypic series from Lengenbach, Binn Valley, Switzerland. *Mineral. Mag.*, **79**, 1089–1098.

Boiocchi, M. & Callegari, A. (2003): Crystal structure refinement of a wallisite–hatchite solid solution. *N. Jb. Miner. Mh.*, **2003**, 396–406.

Brese, N.E. & O'Keeffe, M. (1991): Bond-valence parameters for solids. *Acta Crystallogr.*, **B47**, 192–197.

Brown, K.L. & Dickson, F.W. (1976): The crystal structure of synthetic christite, $HgTlAsS_3$. *Z. Kristallogr.*, **144**, 367–376.

Cai, A. (1984): The substitution of thallium in seligmannite, marrite, laffittite and related mineral phases. *in* "Sulfosalts: observations and mineral descriptions, experiments and applications", G.H. Moh, *et al.* eds. *N. Jahrb. Mineral. Abh.*, **150**, 53–54.

Chakhmouradian, A.R., Mitchell, R.H., Horváth, L. (2007): Rb–Cs-rich rasvumite and sector-zoned "loparite-(Ce)" from Mont Saint-Hilaire (Quebec, Canada) and their petrologic significance. *Eur. J. Mineral.*, **19**, 533–546.

Chen, T.T. & Szymański, J.T. (1981): The structure and chemistry of galkhaite, a mercury sulfosalt containing Cs and Tl. *Can. Mineral.*, **19**, 571–581.

Dmitrieva, M.T., Ilyukhin, V.V., Bokii, G.B. (1979): Close packing and cation arrangement in the djerfisherite structure. *Sov. Phys. Crystallogr.*, **24**, 683–685.

Gagarin, G. & Cuomo, J.R. (1949): Algunas proposiciones sobre nomenclatura mineralogica. *Commun. Inst. Nac. Invest. Cienc. Nat. (Museo argentino cienc. Nat. "Bernardino Rivadavia"), Cienc. Geol., Buenos Aires*, **1**, 1–21.

Graeser, S. & Edenharter, A. (1997): Jentschite ($TlPbAs_2SbS_6$) – a new sulphosalt mineral from Lengenbach, Binntal (Switzerland). *Mineral. Mag.*, **61**, 131–137.

Graeser, S. & Schwander, H. (1992): Edenharterite ($TlPbAs_3S_6$): a new mineral from Lengenbach, Binntal (Switzerland). *Eur. J. Mineral.*, **4**, 1265–1270.

Graeser, S., Cannon, R., Drechsler, E., Raber, T., Roth, P. (2008): Faszination Lengenbach Abbau-Forschung-Mineralien 1958–2008. Kristallographik Verlag, Achberg, Germany.

Hettmann, K., Kreissig, K., Rehkämper, M., Wenzel, Th., Mertz-Kraus, R., Markl, G. (2014): Thallium geochemistry in the metamorphic Lengenbach sulfide deposit, Switzerland: thallium-isotope fractionation in a sulfide melt. *Am. Mineral.*, **99**, 793–803.

Hofmann, B. (1994): Formation of a sulfide melt during Alpine metamorphism of the Lengenbach polymetallic sulfide mineralization, Binntal, Switzerland. *Mineral. Depos.*, **29**, 439–442.

Hofmann, B.A. & Knill, M.D. (1996): Geochemistry and genesis of the Lengenbach Pb–Zn–As–Tl–Ba mineralization, Binn Valley, Switzerland. *Mineral. Depos.*, **31**, 319–339.

Hofmann, B., Graeser, S., Imhof, T., Sicher, V., Stalder, H.A. (1993): Mineralogie der Grube Lengenbach, Binntal, Wallis. *Jahrb. Naturhistorischen Museums Bern*, **11**, 3–90.

Johan, Z., Mantienne, J., Picot, P. (1981): La chabournéite, un nouveau minéral thallifère. *Bull. Minéral.*, **104**, 10–15.

Kasatkin, A.V., Nestola, F., Agakhanov, A.A., Škoda, R., Karpenko, V.Y. & Tsyganko, M.V. (2016): Vorontsovite, IMA 2016-076. CNMNC Neswletter No. 34, December 2016, page 1319. *Mineral. Mag.*, **80**, 1315–1321.

Kraus, W. & Nolze, G. (1996): PowderCell – a program for the representation and manipulation of crystal structures and calculation of the resulting X-ray powder patterns. *J. Appl. Crystallogr.*, **29**, 301–303.

Krenner, J. (1894): A lorándit, új ásványfaj. *Mat. Természettudományi Értesitö*, **12**, 473–473.

Laroussi, A., Moëlo, Y., Ohnenstetter, D. (1989): Silver and thallium in sulfosalts of the sartorite series (Lengenbach, Binn Valley, Switzerland). *C. R. Acad. Sci. Paris Sér. II*, **308**, 927–933.

Makovicky, E. (1997): Modular crystal chemistry of sulphosalts and other complex sulphides. *EMU Notes Mineral.*, **1**, 237–271.

— (2005): Micro- and mesoporous sulfide and selenide structures. *Rev. Mineral. Geochem.*, **57**, 403–434.

Makovicky, E. & Balić-Žunić, T. (1999): Gillulyite $Tl_2(As, Sb)_8S_{13}$: reinterpretation of the crystal structure and order–disorder phenomena. *Am. Mineral.*, **84**, 400–406.

Makovicky, E., Johan, Z., Karup-Møller, S. (1980): New data on bukovite, thalcusite, chalcothallite and rohaite. *N. Jb. Mineral. Abh.*, **138**, 122–146.

Marumo, F. & Nowacki, W. (1967): The crystal structure of hatchite, $PbTlAgAs_2S_5$. *Z. Kristallogr.*, **125**, 249–265.

Matsushita, Y. & Takéuchi, Y. (1994): Refinement of the crystal structure of hutchinsonite, $TlPbAs_5S_9$. *Z. Kristallogr.*, **209**, 475–478.

Moëlo, Y., Makovicky, E., Mozgova, N.N., Jambor, J.L., Cook, N., Pring, A., Paar, W.H., Nickel, E.H., Graeser, S., Karup-Møller, S., Balić-Žunić, T., Mumme, W.G., Vurro, F., Topa, D., Bindi, L., Bente, K., Shimizu, M. (2008): Sulfosalt systematics: a review. Report of the sulfosalt sub-committee of the IMA Commission on Ore Mineralogy. *Eur. J. Mineral.*, **20**, 7–46.

Nestola, F., Guastoni, A., Bindi, L., Secco, L. (2009): Dalnegroite, $Tl_{5-x}Pb_{2x}(As,Sb)_{21-x}S_{34}$, a new thallium sulphosalt from Lengenbach quarry, Binntal, Switzerland. *Mineral. Mag.*, **73**, 1027–1032.

Nickel, E.H. & Grice, J.D. (1998): The IMA commission on new minerals and mineral names: procedures and guidelines on mineral nomenclature, 1998. *Can. Mineral.*, **36**, 913–926.

Nordenskiöld, A.E. (1866): Undersökning af Selenmineralierna från Skrikerum. *Öfv. Kgl. Vet. – Akad. Förhandl.*, **23**, 361–367.

Nowacki, W. (1965): Über einige Mineralfunde aus dem Lengenbach (Binnatal, Kt. Wallis). *Ecl. Geol. Helv.*, **58**, 403–406.

Nowacki, W., Iitaka, Y., Bürki, H. (1960): Structural investigations on sulfosalts from the Lengenbach, Binn Valley, Switzerland. *Acta Crystallogr.*, **13**, 1006–1007.

Orlandi, P., Biagioni, C., Bonaccorsi, E., Moëlo, Y., Paar, W.H. (2012): Lead-antimony sulfosalts from Tuscany (Italy). XII. Boscardinite, $TlPb_4(Sb_7As_2)_{\Sigma 9}S_{18}$, a new mineral species from the Monte Arsiccio mine: occurrence and crystal structure. *Can. Mineral.*, **50**, 235–251.

Orlandi, P., Biagioni, C., Moëlo, Y., Bonaccorsi, E., Paar, W.H. (2013): Lead-antimony sulfosalts from Tuscany (Italy). XIII. Protochabournéite, $\sim Tl_2Pb(Sb_{9-8}As_{1-2})_{\Sigma 10}S_{17}$, from the Monte Arsiccio mine: occurrence, crystal structure and relationship with chabournéite. *Can. Mineral.*, **51**, 475–494.

Oxford Diffraction (2006): CrysAlis RED (Version 1.171.31.2) and ABSPACK in CrysAlis RED. Oxford Diffraction Ltd., Abingdon, Oxfordshire, England.

Pekov, I.V. & Agakhanov, V.V. (2008): Thallium-rich murunskite from the Lovozero pluton, Kola Peninsula, and partitioning of alkali metals and thallium between sulfide minerals. *Geol. Ore Depos.*, **50**, 583–589.

Pekov, I.V., Zubkova, N.V., Lisitsyn, D.V., Pushcharovsky, D.Yu. (2009): Crystal chemistry of murunskite. *Dokl. Earth Sci.*, **424**, 139–141.

Roth, P., Raber, T., Drechsler, E., Cannon, R. (2014): The Lengenbach quarry, Binn Valley, Switzerland. *Mineral. Rec.*, **45**, 157–196.

Sheldrick, G.M. (2015): Crystal structure refinement with SHELXL. *Acta Crystallogr.*, **C71**, 3–8.

Smith, G.F.H. & Prior, G.T. (1907): Red silver minerals from the Binnenthal, Switzerland. *Mineral. Mag.*, **14**, 283–307.

Solly, R.H. (1905): Some new minerals from the Binnenthal, Switzerland. *Mineral. Mag.*, **14**, 72–82.

Solly, R.H. & Smith, G.F.H. (1912): Hatchite, a new (anorthic) mineral from the Binnenthal. *Mineral. Mag.*, **16**, 287–289.

Takéuchi, Y. & Ohmasa, M. (1968): The crystal structure of wallisite, $PbTlCuAs_2S_5$, the Cu analogue of hatchite $PbTlAgAs_2S_5$. *Z. Kristallogr.*, **127**, 349–365.

Topa, D. & Makovicky, E. (2016): Argentobaumhauerite: name, chemistry, crystal structure, comparison with baumhauerite, and position in the Lengenbach mineralization sequence. *Mineral. Mag.*, **80**, 819–840.

Topa, D., Graeser, S., Makovicky, E., Stanley, C. (2016a): Argentoliveingite, IMA 2016-029. CNMNC Newsletter No. 32, August 2016, page 920. *Mineral. Mag.*, **80**, 915–922.

Topa, D., Stoeger, B., Makovicky, E., Stanley, C. (2016b): Incomsartorite, IMA 2016-035. CNMNC Newsletter No. 33, October 2016, page 1136. *Mineral. Mag.*, **80**, 1135–1144.

Topa, D., Makovicky, E., Stanley, C., Cannon, R. (2016c): Argentodufrénoysite, IMA 2016-046. CNMNC Newsletter No. 33, October 2016, page 1138. *Mineral. Mag.*, **80**, 1135–1144.

Topa, D., Makovicky, E., Stroeger, B., Stanley, C. (2017a): Heptasartorite, $Tl_7Pb_{22}As_{55}S_{108}$, enneasartorite, $Tl_6Pb_{32}As_{70}S_{140}$, and hendekasartorite, $Tl_2Pb_{48}As_{82}S_{172}$, three members of the anion-omission series of 'sartorites' from the Lengenbach quarry at Binntal, Wallis, Switzerland. *Eur. J. Mineral.*, **29**, DOI:10.1127/ejm/2017/0029-2634 (this issue).

Topa, D., Kolitsch, U., Makovicky, E., Stanley, C. (2017b): Écrinsite, $AgTl_3Pb_4As_{11}Sb_9S_{36}$, a new thallium-rich homeotype of baumhauerite from the Jas Roux sulphosalt deposit, Parc National des Écrins, Hautes-Alpes, France. *Eur. J. Mineral.*, **29**, DOI:10.1127/ejm/2017/0029-2639 (this issue).

Wilson, A.J.C., ed. (1992): International Tables for Crystallography, Volume C: Mathematical, Physical and Chemical Tables. Kluwer Academic, Dordrecht, NL.

Yin, W., Feng, K., Kang, L., Kang, B., Deng, J., Lin, Z., Yao, J., Wu, Y. (2014): Syntheses, structures, optical properties, and electronic structures of $KBaMSe_3$ (M = As, Sb). *J. Alloys Compd.*, **617**, 287–291.

Received 14 November 2016
Modified version received 9 March 2017
Accepted 3 April 2017